Microglia involvement in the schizophrenia occurrence in male offspring with maternal dexamethasone exposure

Chan Rim
CHA University, CHA BIO COMPLEX
Hyun-Sun Park
Inje University
Min-Jung You
CHA University, CHA BIO COMPLEX
Bohyun Yang
CHA University, CHA BIO COMPLEX
Hui-Ju Kim
CHA University, CHA BIO COMPLEX
Soyoung Sung
CHA University, CHA BIO COMPLEX
Min-Soo Kwon (minsoo100@cha.ac.kr)
CHA University, CHA BIO COMPLEX

Research Article

Keywords: Microglia, Schizophrenia, Sex-biased behaviors, Prenatal stress, Depression

Posted Date: May 25th, 2022

DOI: https://doi.org/10.21203/rs.3.rs-1676907/v1

Abstract

Background: Fetal microglia are particularly sensitive cells to the changes *in utero* environment and show sex-biased differences in shape and function. Maternal stress hormone induction can affect fetal microglial functions including alterations in synaptic pruning and cytokine secretion. It may contribute to psychiatric outcomes in offspring such as schizophrenia and depression.

Methods: We administered a 50 μg/kg dexamethasone (DEX) to dams subcutaneously from gestational days 16 to 18. To characterize behaviors of maternal DEX exposed offspring, we assessed depressive-like and schizophrenia-relevant behaviors among 5 week old (adolescence), 10 week old (adult), and orchiectomized group respectively. Using quantitative real-time polymerase chain reaction, western blotting, and rapid Golgi staining, microglial morphology and synaptic pruning were assessed.

Results: Prenatal exposure to dexamethasone (PN-DEX) induced SCZ-relevant behavior in male mice and depressive-like behavior in female mice. SCZ-relevant behavioral patterns were induced in 10 week old (10 W) male mice but not in 5 week old (5 W) male mice. Microglia in the medial prefrontal cortex (mPFC) and the striatum (STR) of 10 W males prenatally treated with dexamethasone (10 W PN-DEX-M) showed hyper-ramified morphology and dramatically reduced spine density in mPFC. Immunofluorescence studies indicated that microglia in the mPFC of the 10 W PN-DEX-M group interacted with pre-synaptic Bassoon and post-synaptic density 95 (PSD95) puncta. PN-DEX-M also showed significantly changed dopamine system proteins. A testosterone surge was not observed in parallel to SCZ-relevant behavior in 10 W PN-DEX-M. Furthermore, females prenatally treated with dexamethasone (PN-DEX-F) displayed depressive-like behavior, in addition to HPA axis activation and inflammatory microglial phenotypes in their hippocampus (HPC).

Conclusions: Our study demonstrated that maternal DEX exposure induces sex-biased abnormal behavior as well as SCZ-relevant behavior in male offspring, and depressive-like behaviors in female offspring. We propose that altered microglial function, such as increased synaptic pruning, may be involved in the occurrence of SCZ-relevant behavior in PN-DEX-M and sex-biased abnormal behavior in the PN-DEX model.

Introduction

Schizophrenia (SCZ) is a serious mental illness characterized by psychotic symptoms, cognitive impairment, and functional decline in daily life. Reportedly, less than 1% of the global population suffer from SCZ, the onset of which occurs in early adulthood, following adolescence [1]. Several studies have suggested that SCZ is more common in men than in women [2].

A growing body of research continues to explore the possibility that prenatal stress may act as a risk factor which increases the probability of SCZ onset during adulthood [3]. Several types of stressors, including social defeat, chronic stress, and dexamethasone (DEX), affect neurodevelopment as well as the hypothalamic-pituitary-adrenal axis (HPA axis) and epigenetic landscape, via increased maternal

glucocorticoid (Gc) levels which are transmitted to the fetus through the placenta [4]. However, causal factors that initiate the onset of SCZ as well as mechanisms that underly the sculpting of the vulnerable central nervous system (CNS) by prenatal stress remain unclear.

Microglia are the primary innate immune cells of the CNS. They play an important role in neuron maturation and the maintenance of neuronal homeostasis by establishing contact with neurons [5]. Microglia, which play a dual role by both eliminating excessive synapses and promoting synaptogenesis, act as primary organizers of synapses and neuronal circuits [6]. Extensive research into the role of microglia in synaptic development has indicated that dysfunctional microglia are associated with several neuropsychiatric disorders [7, 8]. With respect to SCZ patients, in particular, excessive pruning of neuronal synapses by microglia results in low synaptic density [9] and abnormal behavior [10, 11]. In humans, synaptic density peaks during adolescence and gradually decreases as adulthood approaches [12]. Thus, excessive reduction of synaptic density induced by biological and/or environmental factors during this process may induce SCZ [13].

The dopamine theory in SCZ propounded by several studies postulates that the dysregulation of two dopaminergic pathways stemming from the ventral tegmental area (VTA), including mesolimbic (midbrain to striatum) and mesocortical (midbrain to the prefrontal cortex), are associated with schizophrenic symptoms [14, 15]. These two dopamine circuits are reportedly vulnerable to stress [16]. The prefrontal cortex (PFC) is known as a stress-sensitive region of the brain [17]. A PFC that is subjected to excessive stress induces an imbalance in the dopamine system [18]. Dysregulation of D1R and D2R (dopamine receptor)-positive GABAergic medium spiny neurons (MSNs) in the striatum (STR) also contributes to the occurrence of SCZ [19]. Interestingly, the dopamine receptors, D1 and D2, localized in both pre-and post-synapses may be regulated via synaptic pruning, but not via synapse formation [20].

Microglia also play a role in sex differentiation in the developing brain [21]. According to a previous study [22], microglia show sex-biased morphological features and neuroinflammation. Additionally, sex-specific transcriptional profiles of microglia have been observed [23, 24]. Thus, exploring sex-bias in microglia may be key to understanding sex-biased psychiatric disorders and their underlying pathophysiologies.

The current study was conducted to elucidate possible mechanisms underlying prenatal stress hormone induction induced SCZ-relevant behavior in mice. To mimic elevated stress hormone levels *in vivo*, we administered dexamethasone (DEX), a synthetic glucocorticoid, to female mice during late pregnancy. We found that prenatal DEX exposure (PN-DEX) evoked SCZ-relevant behavior in male offspring after adolescence while inducing depressive-like behavior in female offspring.

Materials And Methods

Experimental animals

Male and female C57BL/6 mice (Koatec Inc., Korea) used in all experiments were housed in cages holding 3 ~ 5 animals each, under specific pathogen free (SPF) conditions at 22 ± 0.5°C and an

alternating 12-h light-dark cycle at the CHA BIO COMPLEX animal facility (Seongnam, Korea), and supplied with food and water ad libitum. The animals were acclimatized to the laboratory for 1 week before being subjected to experiments. In order to reduce time dependent variability, all experiments were performed during the light phase of the cycle. All experimental animals were handled in accordance with the guidelines of the Institutional Animal Care and Use Committee of CHA University (IACUC2100037).

Prenatal Dexamethasone (DEX) Treatment

The experimental model described by Nagano et al., (2008) was adopted with some modifications [25]. In brief, to mimic the induction of stress hormones during the prenatal period, a dose of 50 μg/kg dexamethasone (DEX, Sigma D1756, USA) or physiological saline was injected subcutaneously into pregnant mice once a day from gestational day (GD) 15 to 17. The dose of DEX needed was determined by taking the physiological glucocorticoid levels induced by stress conditions estimated by a previous study of ours [26] into consideration. Two days after birth, pups were randomly assigned to each experimental group. After the weaning period, the pups were categorized into 3–5 animals per cage based on their sexes.

Behavioral tests

The mice were allowed to acclimatize to the testing room for at least 30 min before performing assessments. A previous study [25], indicated that DEX may induce behavioral changes in the offspring of DEX-injected mice, 10 d after birth. Therefore, all behavioral assessments were conducted during the light cycle (between 9:00 AM and 7:00 PM) from 11 to 16 weeks after birth. To assess anxiety/depressive-related behavior in mice, we conducted an open field test (OFT), a light/dark exploration (LD), a tail suspension test (TST), a forced swim test (FST), and a sucrose preference test (SPT). Furthermore, in order to examine social behavior, we conducted a three-chamber social interaction (SI) test. Latent inhibition (LI), and prepulse inhibition (PPI) tests were performed to assess schizophrenia-related behavior. These behavioral assessments were conducted in series. Depending on the experimental design, the order of these behavioral assays were slightly changed. Each assessment was conducted during a single day, as described in our previous studies [27]. The observers were blinded to the groups, and the data so obtained were compared by two observers to minimize bias.

The open field test

Mice were placed in a 50×50 cm white Plexiglas box which was brightly lit using fluorescent room lighting; six 60 W incandescent bulbs were placed 4–6 feet above the box. Activity was recorded using a ceiling-mounted video camera and analyzed using EthoVision software (Noldus, Leesburg, VA). This software displays the paths taken by mice and measures the total distance moved and the number of entries into the center of the arena (central 17 cm square) during a 10 min session.

Light dark exploration

The apparatus used in this assessment was a box (30×30×30 cm) consisting of one brightly lit open chamber connected to a darkened, enclosed chamber. The chambers were connected by a small square hole (7 ×7 cm). Mice were placed in the corner of the lit chamber, facing away from the dark chamber, and the time spent in the dark chamber during a period of 10 min was manually measured.

Tail suspension test

The apparatus consisted of a cupboard with a hook attached to the top. Mice were suspended by securing the tail to the hook with adhesive tape which was wrapped around the tail. The tail was carefully suspended so as not to bend it, by keeping the tip of the tail 2 cm away from the top of the hook. Data pertaining to mice that climbed their tails were excluded. The time spent immobile during the 7 min testing period was measured by three observers who were blinded to the groups.

Forced swim test

Each mouse was placed in a 2 L Pyrex beaker (13 cm diameter, 24 cm height), which was filled with 24°C water to a depth of 17 cm, and forced to swim for 6 min. The duration of immobility was measured during the final 5 min of the test. Immobility was defined as the time each mouse spent floating without struggling and only making movements that were necessary to keep its head above water level. The time spent immobile during the 5 min testing period was measured by three blinded observers.

Three-chamber social interaction

The social interaction box was a rectangular, three-chambered box made of white Plexiglas (60 cm × 40 cm × 40 cm). Each chamber measured 20 cm × 40 cm × 40 cm. Dividing walls were also made of clear Plexiglas with a small opening (square, 6 cm × 6 cm) that allowed access to each chamber. Each test mouse was placed in the middle chamber and allowed to explore for 5 min. The doorways in the two side chambers were blocked with plastic boxes during the habituation phase. After 5 min of habituation, an unfamiliar mouse of the same strain, that had no prior contact with the subject mouse, was placed in one side chamber. The location of the stranger mouse was systematically alternated between the left- and right-chambers during the trial. The stranger mouse was enclosed in a cylinder made of transparent Plexiglas, which allowed nose contact through the holes, but prevented fighting. The cylinder was 15 cm in height, with a bottom diameter of 8 cm and holes spaced 1 cm apart. The cover, made of Plexiglas, was placed on top of the cylinder to prevent the test mouse from climbing ,also prevent the stranger mouse from escaping. Both doors to the side chambers were then unblocked, and the test mouse was allowed to explore the entire social interaction box for a 10-min session to measure sociality. Activity in the social interaction chamber was recorded, and the time spent in each chamber was measured using an EthoVision XT9 video tracking system. After the first 10 min session ended, each mouse was tested in a second 10-min session to check social preference for a new stranger, using a second unfamiliar mouse, which was also enclosed in a cylinder made of transparent Plexiglas, and placed in the chamber that had been empty during the first 10-min session. The test mouse had a choice between the first, already-investigated, unfamiliar mouse (stranger 1) and the second, unfamiliar mouse (stranger 2). As described

above, the activity in the social interaction chamber was recorded, and the time spent in each chamber was measured using an EthoVision XT9 video tracking system.

Latent inhibition

This protocol was modeled after a previous study [28]. Each mouse group (control or amphetamine) was randomly subdivided into two groups: pre-exposed (PE); and non-pre-exposed (NPE). The mice were placed in a shuttle box (Jungdo Biotech, Seoul, Korea) with a speaker mounted on the back wall. PE mice were exposed to 40 tones (1 tone; 2000 HZ, 30 s duration) separated by 30 ± 40 s to randomize the inter-tone interval. The NPE mice were placed in the same enclosure for an equivalent amount of time. Immediately following pre-exposure, all mice were given three pairing trials of the 30 s tone, followed immediately by a 1 s, 0.3 mA foot-shock delivered through the floor. Pairing trials were separated by 180 s. Mice were returned to the enclosure the next day and presented with an 8 min tone presentation following a 180 s acclimation period. Freezing during tone presentation was measured using EthoVision XT9. The percentage of time spent freezing during tone presentation was measured, with LI being defined as the difference between the amounts of freezing in response to the tone by PE mice and NPE mice. The NPE groups were merged to obtain greater statistical power.

Acoustic startle/Prepulse inhibition

PPI testing, which adopted the method described by Dulawa et al.,(2000) with modifications, was performed in SR-LAB startle chambers (San Diego Instruments, San Diego, CA). Mice were exposed to 5 different types of discrete stimuli or “trials” as follows: a 40-msec broadband 120 dB burst (Pulse Alone trial); 3 different Prepulse + Pulse trials in which either 20-msec long 3 dB, 6 dB or 12 dB above background stimuli preceded the 120 dB pulse by 100 msec (onset to onset); and a No Stimulus trial, during which only background noise was presented. The trials were conducted in a pseudo-random order, separated by an average of 15 s (range,7–23 s). The test session began with a 5-min acclimation period, followed by four consecutive blocks of test trials. Blocks 1 and 4 consisted of six consecutive Pulse Alone trials, while blocks 2 and 3 each contained six Pulse Alone trials, five of each type of Prepulse + Pulse trials, and five No Stimulus trials. Thus, the entire 22-min session consisted of 62 test trials. PPI was calculated as follows: [100 – (Prepulse-Pulse trial/Pulse alone) × 100]. The pulse-alone trials in this calculation involved the averaged pulse-alone values for blocks 2 and 3.

Immunofluorescence

For perfusion purposes, the mice were sacrificed following behavioral assessment. The mice were deeply anesthetized using sodium pentobarbital (100 mg/kg, i.p.) and perfused intracardially with heparinized saline, followed by ice-cold phosphate-buffered 4% paraformaldehyde (pH 7.4). Each brain was dissected and post-fixed in the same fixative at 4°C. Next, brain blocks were cryoprotected in 30% sucrose for 24 h at 4°C, following which 25 mm thick sections were obtained using an electronic cryotome (Leica CM 3050S, Germany). Sections were first rinsed thrice (10 min each time) with 1% bovine serum albumin (BSA) in 0.1 M phosphate buffered saline (PBS). For permeabilization and blocking purposes, the tissues were pre-incubated in 0.1 M PBS containing 10% Bovine serum albumin (BSA; Roche, 10735086001), 3%

Fetal bovine serum (FBS; Gibco, USA, 16000-044), 5% Normal donkey serum (NDS), and 0.3% Triton X-100 for 1 h at room temperature (RT). After rinsing twice (10–15 min each time) with 0.1 M PBS containing 0.5% BSA, sections were incubated with polyclonal anti-rabbit anti-Iba-1 antibodies (1:500; Wako, Japan # 019-19741), goat anti-Iba-1 antibodies (1:500; Novus, USA, #NB100-1028), mouse anti-Bassoon antibodies (1:1000; Novus, #NB120-13249), and rabbit anti-PSD95 (1:500; Abcam, UK, #ab238135) diluted with 0.1 M PBS containing 0.5% BSA at RT. Following overnight incubation, sections were rinsed and incubated with Alexa-488 conjugated anti-rabbit IgG antibodies (Invitrogen, USA, A21206), Alexa-488 conjugated anti-goat IgG antibodies (Invitrogen, A11055, Alexa-594 conjugated anti-rabbit IgG antibodies (Invitrogen, A21207), and Alexa-647 conjugated anti-mouse IgG antibodies (Invitrogen, A31571) in a 1:200 dilution with 0.1 M PBS containing 1% BSA for 1 h at RT. After rinsing with 0.1M PBS, coverslips were mounted using Prolong™ Gold antifade mounting solution with DAPI (Invitrogen, P36931).

Microglia and synaptic protein colocalization

Bassoon and Post-synaptic density protein 95 (PSD95) puncta, as well as pre-and post-synaptic markers, which were colocalized with Iba-1 positive cells, respectively, were analyzed using Huygens professional software for Mac (Scientific Volume Imaging, Netherlands) and Image J (National Institutes of Health, Bethesda, MD, USA). Briefly, z-stacked confocal images (1 μm slices) were converted to maximum-intensity projection images using ImageJ software. In order to obtain clear and noise-reduced images, we conducted a deconvolution process using Huygens professional software. Next, a colocalization analysis tool with identical threshold settings was used throughout the study; 6–10 Iba-1 positive cells per mouse (3 mice per group) were analyzed.

Microglial cell morphometrics

Skeletal and Sholl analysis

Microglial morphology was analyzed according to a previously described method [29]. In brief, z-stacked confocal images (1 μm slices) were converted to maximum intensity projection images using ImageJ. To exclusively visualize positive staining, an unsharp mask filter was applied to stacked images and brightness and contrast was adjusted. Next, RGB images were converted to grayscale images, and a threshold was applied. To obtain clear and precise images, noise reduction techniques, such as removing outliers and de-speckling, was applied to binary images, followed by skeletonizing branches. Lastly, the analyze skeleton plugin was run and data was trimmed to remove skeleton fragments using Microsoft Excel. Endpoints/cells and branch length/cells were calculated manually. The size of microglia in the regions of interest (ROIs) was manually calculated using the freehand tool in ImageJ software. A total of 200 to 300 microglial cells per group (3 mice, 5–6 fields per group) were used for skeletal analysis. Single microglia in the 8-bit and z-stacked images were isolated by removing surrounding artifacts and other cell fragments via the eraser tool, which was originally built into ImageJ. The experimenter then drew a straight line from the center of the microglial soma to its longest branches using the line segment tool. Finally, using the Sholl analysis plugin, the first shell was defined as 10 μm outside the cell body, and each step was set to 5 μm. The number of microglial branch intersections was automatically calculated

using the Sholl analysis plugin. Fifteen single microglia per mouse (3 mice per group) were randomly selected and analyzed.

Western Blot

Proteins in the medial prefrontal cortex (mPFC), striatum (STR), and the hippocampus (HPC) were extracted, and their expression levels assessed using western blotting. After dissecting, the mPFC, STR, and HPC, tissues were lysed with RIPA buffer (Sigma #R0278) and homogenized. To obtain pure proteins, debris was removed by ultracentrifugation following whole tissue homogenization. Protein concentrations were determined using a detergent-compatible protein assay reagent (Bio-Rad Laboratories, USA) with BSA as the standard. After adding dithiothreitol (5 mM) and bromophenol blue (0.1% w/v), the proteins were boiled, separated by electrophoresis on 10–15% polyacrylamide gels (Invitrogen), and transferred onto polyvinylidene difluoride (PVDF) membranes (Bio-Rad Laboratories). The membranes were blocked on a shaker for 1 h at RT with Tris-buffered saline/0.1% Tween-20 (TBS-T) and 5% nonfat dry milk. Primary antibodies were dissolved in the blocking buffer and the membranes were immunoblotted with antibodies against dopamine receptor D2 (DRD2; 1:200, Bioss #bs-1008R), dopamine transporter (DAT; 1:200, Abcam #ab111468), tyrosine hydroxylase (1:200, Abcam #ab112), post-synaptic density 95 (PSD95; 1:500, Abcam #ab18258), synaptophysin (Physin; 1:5000, Abcam, #ab14692), glucocorticoid receptor (GR; 1:1000, Santa Cruz Biotechnology, USA, #SC1004), 5-HT1a receptor (5-HT1aR; 1:1000, GeneTex, USA, # GTX104703), brain-derived neurotrophic factor (BDNF; 1:1000, Abcam #ab108319), CX3C chemokine receptor1 (CX3CR1; 1:1000, Abcam #ab8021), Arginase 1 (ARG1; 1:2000, Novus #NB100-59740), cAMP response element-binding protein (CREB; 1:500, Cell Signaling Technology # 9197S), XXXhosphor-CREB (pCREB; 1:500, Cell Signaling Technology, USA, #9198S) and beta-actin (1:5000, Cell Signaling #4970S). The membranes were incubated in)oat anti-rabbit (1:10000, Enzo #ABI-SAB-300-J) or goat anti-mouse (1:10000, BETHYL, A120-101P) antibodies and dissolved in blocking buffer at room temperature for 1 h. The membranes were visualized using an ECL-plus solution (GE Healthcare, USA, RPN2106V1 and V2), following which they were exposed to chemiluminescence (LAS-4000; Fujifilm, Japan) to detect light emission. Western blot results were quantified using ImageJ 1.51 software (National Institutes of Health, Bethesda, MD, USA) following densitometric scanning of films.

Quantitative Real-time Polymerase Chain Recation (qRT-PCR)

Following behavioral assessments, the mPFC, STR, and HPC were dissected to analyze mRNA expression. To extract RNA, frozen tissue was homogenized in 1 mL of TRIzol reagent per 100 mg of tissue (Life Technologies, 15596018). Chloroform was added to separate phase-containing RNA, while isopropyl alcohol was added to precipitate RNA. Each precipitated RNA pellet was air-dried and dissolved in DEPC-treated water (Life Technologies; AM9906). RNA concentration was determined by measuring absorption at 260 nm. Messenger RNA (mRNA) was reverse-transcribed into cDNA in 20 µL of reaction mix using a RevertAid First Strand cDNA Synthesis Kit (ThermoFisher Scientific, K1622). Quantitative PCR was performed using Power SYBR® Green PCR Master Mix (Life Technologies, 4367659). Primer

sequences are listed (Table S1). Cyclic conditions consisted of initial enzyme activation at 95°C for 5 min, followed by 50 cycles of denaturation at 95°C for 20 s, annealing, and extension, including detection of SYBR Green bound to PCR product at 56°C for 40 s. Glyceraldehyde 3-phosphate dehydrogenase (GAPDH) was used as an internal control for normalization. Relative quantities of PCR fragments were calculated using the comparative CT method.

Golgi Staining

To determine synaptic density, we performed Golgi staining using a FD Rapid GolgiStain™ kit (FD NeuroTechnologies, Columbia, MD, USA) according to the manufacturer's protocols. Briefly, mice were euthanized and their brains perfused with heparinized double physiological saline. The brains were then immersed in solutions A and B for the impregnation step and stored at room temperature for up to 2 weeks in the dark. Next, the brains were transferred to solution C, following which 4 were stored in the dark for up to one week. Each brain was serially sectioned at a thickness of 100 μm using a cryotome (Leica Biosystems, Germany). The sections were mounted on gelatin-coated slides and allowed to dry naturally at room temperature. Mounted sections were rinsed with double-distilled water and allowed to react with an equal volume of solutions D and E in the dark for 10 min. Next, sections were rinsed in double-distilled water and dehydrated via an ascending alcohol gradient (50, 75, 80, 95, and 100%). After dehydration, the sections were cleaned in Histoclear (National Diagnostics, Georgia, USA) and cover-slipped with Permount solution (Fisher Chemicals #SP15-500 HS200). Dendritic spines were observed under a Zeiss Axioscan z1 microscope (Zeiss, Germany). Spine density and dendrite length were quantitatively analyzed by counting spines and dendrites using SynPAnal software [30]. The experimenters were blinded to the groups and 10 dendrites per mouse were selected for further analyses.

Enzyme-linked immunosorbent assay (ELISA)

Mice were sacrificed, following which whole blood was collected via cardiac puncture, and serum was isolated and stored at − 80°C until assayed. Serum glucocorticoid and testosterone levels were determined using a corticosterone ELISA kit (Enzo, #ADI-900-097) and a testosterone ELISA kit (Enzo #ADI-900-065), respectively, according to the manufacturer's instructions.

Statistical analysis

Data are presented as mean ± standard error of the mean (SEM). Significance of the differences between groups was assessed via unpaired Student's t-tests and two-way analysis of variance (ANOVA) followed by Tukey's post-hoc test, using GraphPad Prism version 7 for Mac (GraphPad, La Jolla, CA). Statistical significance was set at $p < 0.05$.

Results

Maternal dexamethasone (DEX) exposure induces different, sex-dependent, a*bnormal behaviors in offspring.*

To investigate the effect of maternal stress hormone induction on fetal microglia *in vivo*, we administered a synthetic glucocorticoid (DEX) to dams. Considering that the gestation period of a mouse lasts between 19–21 d, and that approximately 15–21 d mark the end of the trimester, DEX was administered subcutaneously once a day for 3 d from gestational days (GDs) 16 to 18 to induce consistent exposure of all fetuses to DEX. Determination of the dose (50 μg/kg) to be administered was based on the findings of a previous study [25] as well as the estimated physiological concentration of glucocorticoids under stressful situations [26]. Pups were separated according to sex following lactation. The number of litters of each pregnant dam was counted after parturition, and no significant differences in litter size or sex-bias between the Veh and PN-DEX groups was observed (Fig. S1a-b). In addition, there were no significant differences between the body weights of adult PN-DEX and Veh mice (Fig. S1c).

Next, a series of behavioral assessments of PN-DEX offspring were conducted. The offspring were examined during their adolescent (5-week-old: 5 W) and adult (10-week-old: 10 W) stages (Fig. 1a). The 5 W PN-DEX-M did not exhibit depressive-like behavior or schizophrenia-relevant behavior, during TST, SPT, or PPI (Fig. 1b-d). However, results of the TST showed that the immobile time of 5 W PN-DEX-F was increased (Fig. 1b), although those of SPT, PPI, or SI did not show any significant changes (Fig. 1c-d; Fig. S1d-e). The results of both TST and FST indicated that the immobile time of 10 W PN-DEX-F was increased in a manner similar to that of 5 W PN-DEX-F, while that of the LD test showed that time spent in the dark zone by 10 W PN-DEX-F was longer compared to that of 10 W Veh-F (Fig. 1e-h). The 10 W PN-DEX-F group did not show any significant changes in SPT, OFT, and SI (Fig. 1i, Fig. S1e-i). This suggested that exposure to PN-DEX induced depressive-like behaviors in the 5 W PN-DEX-F group, which behavior continued until the adult stages. Although the PN-DEX-F group showed depressive-like behavior, the PN-DEX-M group did not (Fig. 1e-i, Fig. S1f-i).

Interestingly, we found that, as opposed to the 5 W PN-DEX-M group, the 10 W PN-DEX-M group exhibited some major characteristics of the animal schizophrenia model, such as significant impairment of prepulse inhibition and latent inhibition, whereas the 10 W PN-DEX-F group did not (Fig. 1j-l). Locomotor activity after being injected with the psychotropic drug, amphetamine (AMP), was measured to verify experimental results. The 10 W PN-DEX-M group showed increased locomotor activity following AMP treatment, compared with that of the Veh group (Fig. 1m-n).

Change of microglia morphology and gene expression in male offspring with maternal dexamethasone exposure

First, we investigated factors that contribute to schizophrenia-relevant behavior in 10 W PN-DEX-M mice. At puberty, the number of dendritic spines in the gray matter of the human and non-human mPFC is decreased due to synaptic pruning [31]. Therefore, we hypothesized that schizophrenia-relevant behavior seen in 10 W PN-DEX-M may have been mediated by microglia.

We analyzed changes in the microglial morphology of 5 W and 10 W PN-DEX-M groups. To precisely depict morphological changes in microglia, we selected two different but widely used methods, and

modified the pipelines to suit our experimental environment. First, we conducted a 2D skeletonization [32]. First of all, microglial numbers both in mPFC and STR were not changed by maternal DEX exposure (Fig. S2a-d). There was no significant change in endpoints, or average branch lengths in the mPFC of the 5 W PN-DEX-M group compared to that of the 5 W VEH-M group. By contrast, the mPFC of the 10 W PN-DEX-M showed enlarged microglial soma, increased endpoints, and average branch lengths (Fig. 2a-b). Interestingly, these changes were not found in the microglia of the 5 W and 10 W PN-DEX-F groups (Figs. S3a-c and S4a-c). Secondly, to verify increased microglial ramification, we conducted a Sholl analysis, which assesses the complexity of cellular branches [33]. The Microglial Sholl analysis revealed that the increased number of intersections in the microglia of the 10 W PN-DEX-M group was increased (Fig. 2c). By contrast, there were no significant differences between either 5 W PN-DEX-F and Veh-F groups or between 10 W PN-DEX-F and Veh-F groups (Fig. S3d and S4d). These results indicated that the mPFC of the PN-DEX-M group had undergone morphological changes to a hyper-ramified state after adolescence, compared to that of the Veh-M group.

Next, we analyzed microglial signature genes and functional regulators involved in neuronal interactions in the mPFC. In particular, Cx3cr1, which is related to microglia-neuron contact and microglial migration, was greatly increased in the 10 W PN-DEX-M group compared to 10 W Veh-M. With respect to cytokines, Il-1 beta expression remained unchanged, but Il-6 and TNF-α were significantly decreased in 10 W PN-DEX-M. On the other hand, anti-inflammatory genes, such as *Il-10*, and *Arg-1* were highly increased only in 10 W PN-DEX-M (Fig. 2h). Neither 5 W PN-DEX-M (Fig. 2g), nor 5 W or 10 W PN-DEX-F showed such changes (Figs. S3e and S4e).

We also analyzed microglial morphology and gene expression in the striatum, a region that is functionally related to the prefrontal cortex [34]. There were no significant changes between the morphologies of striatal microglia in the 5 W Veh-M and 5 W PN-DEX-M groups (Fig. 2d-f), or the 5 W PN-DEX-F group (Fig. S3f-i). Microglial signature genes and cytokine genes in the 5 W PN-DEX-M group remained unchanged, except for the mRNA expression of *Arg1* (Fig. 2j). However, morphology of the microglia in the striatum of the 10 W PN-DEX-M group changed to a hyper-ramified state similar to that of the microglia of the mPFC. Although the size of their soma did not increase, the endpoint number and average branch length of the striatal microglia of the 10 W PN-DEX-M group increased, (Fig. 2d-f), as opposed to those of 10 W PN-DEX-F, which did not (Fig. S4f-i). In addition, the gene expression patterns in the striatum of 10 W PN-DEX-M were different from those in its mPFC. In the striatum of 10 W PN-DEX-M, *Trem2*, which is the regulator of the phagocytic function of microglia, was decreased, while *Cx3cr1* and *Il-6* were increased (Fig. 2j). Interestingly, there were no significant changes in gene expression in the striatum of 5 W PN-DEX-F mice, except for that of *Arg-1* (Fig. S3j). On the other hand, expression of *C1qa* and *C3ar1*, which encode complement proteins and their receptors, respectively, as well as the expression of *Cx3cr1* were decreased in 10 W PN-DEX-F (Fig. S4j).

Involvement of microglia on synaptic density and dopamine system in male offspring with maternal dexamethasone exposure

Dopamine signaling in the mPFC is associated with higher mental functions involving cognitive, emotional, and motivational processes [35, 36]. In the mPFC of 10 W PN-DEX-M mice, the expression of factors that facilitate dopamine synthesis and transport, including dopamine receptor D2 (DRD2), dopamine transporter (DAT), and tyrosine hydroxylase (TH), were slightly decreased (Fig. 3d-e). In addition, synaptophysin and post-synaptic density protein 95 (PSD95) as well as pre-and post-synaptic proteins in 10 W PN-DEX-M were also slightly decreased (Fig. 3d-f). Conversely, although dopamine-related protein levels in the striatum of 10 W PN-DEX-M were significantly increased, synaptic protein levels were not (Fig. 3j-l). These data indicated that prenatal DEX exposure induced an imbalance in the cortico-striatal dopaminergic pathway as well as an aberrant synaptic protein expression pattern in 10 W PN-DEX-M. Interestingly, no significant changes were observed in the expression of synaptic and dopamine-related proteins in the mPFC or the striatum of 5 W PN-DEX-M (Figs. 3a-c and 3g-i). Furthermore, there were no significant changes in dopamine-related proteins and synaptic proteins in either region of 5 W and 10 W PN-DEX-F, except for a decrease in DAT expression observed in the mPFC of 5 W PN-DEX-F (Figs. S3k-l and S4k-l). A recent study reported that the microglial dopamine receptor (DR) is associated with synapse elimination [37]. Therefore, we hypothesized that microglial changes may lead to the dysregulation of synaptic pruning and the dopamine system, and thus performed rapid Golgi staining to visualize synaptic spines in the mPFC and striatum. No changes were observed in the spine densities of both the mPFC and the striatum of 5 W PN-DEX-M, compared to those of 5 W Veh-M (Figs. 4a-b; 4d-e). By contrast, spine density in the mPFC of 10 W PN-DEX-M, was dramatically reduced, while that in the striatum was not (Figs. 4a,c; 4d,f). Considered together, these findings indicated that prenatal DEX exposure affects spine density as well as the dopamine system in the mPFC and striatum of adult male offspring. With respect to morphological changes in the microglia of the 10 W PN-DEX-M group, we hypothesized that microglia may be responsible for the decrease seen in the synaptic density of the mPFC. In order to verify this, we calculated Bassoon (a pre-synaptic marker) and PSD95 (a post-synaptic marker) puncta colocalized with IBA1 positive cells (Fig. 4g). In line with our Golgi staining and western blot results, we found significantly increased pre-synaptic Bassoon and post-synaptic PSD95 puncta colocalized with IBA1 positive cells in the mPFC of the 10 W PN-DEX-M group, compared to those of the 10 W Veh-M group (Fig. 4h-i). These data indicated that maternal DEX exposure may affect microglia-mediated synaptic elimination between adolescence and adulthood.

Testosterone surge in adolescence is not related to the occurrence of schizophrenia-relevant behaviors in male offspring with maternal DEX exposure

The above results indicated that maternally DEX-exposed male offspring may experience the onset of SCZ-relevant behavior in early adulthood (10 W), after adolescence (5 W). Sex hormonal changes are the main events associated with adolescence, wherein testosterone acts as a determinant factor that produces maleness. Thus, we hypothesized that sex-biased biological events, such as testosterone surge may evoke SCZ-relevant behavior in PN-DEX-M, by inducing microglial changes after adolescence. To verify this speculation, we orchiectomized (Orx) 4 W PN-DEX-M to inhibit the testosterone surge and then performed PPI (Fig. 5a). The testes, epididymis, and the vas deferens were dissected (Fig. 5b). Orchiectomy decreased the serum testosterone levels in male mice to an extent which paralleled that of

age-matched females (Fig. 5c). However, orchiectomy did not rescue impaired PPI in the PN-DEX-M group (Fig. 5f). By contrast, PN-DEX-Orx did not exhibit depressive-like behavior (Fig. 5c-e). In conclusion, the occurrence of SCZ-relevant behavior in the 10 W PN-DEX-M group was not due to the testosterone surge that occurs around puberty.

PN-DEX-F showed HPA axis activation and inflammatory microglia phenotype in the hippocampus (HPC)

To determine whether depressive-like behavior in PN-DEX-F is accompanied by molecular changes in the brain, we examined HPA axis-related factors, including hypothalamic corticotrophin-releasing hormone (CRH) and serum glucocorticoids (Gc). The 10 W PN-DEX-F group showed increased hypothalamic Crh levels and serum Gc levels compared to those of 10 W Veh-F (Figs. 6a-b), in accordance with which, hippocampal glucocorticoid receptor (GR) expression was decreased (Fig. 6c). This indicated that 10 W PN-DEX-F underwent HPA activation and GR resistance. Moreover, 10 W of PN-DEX-F showed a slight decrease in CX3CR1 and Arg-1 protein expression (Fig. 6c).

Furthermore, we analyzed the morphology of HPC microglia. The number of microglia in the 10 W PN-DEX-F, group was decreased (Fig. 6d-e), in addition to which microglial somas were enlarged and displayed decreased branch arborization and branch lengths (Fig. 6f-h). The de-ramification of HPC microglia was confirmed by Sholl analysis (Fig. 6i). Moreover, the mRNA expression levels of the pro-inflammatory cytokines, Il1-beta, Il-6, and Tnf-alpha, in the 10 W PN-DEX-F group were increased compared to those in 10 W Veh-F (Fig. 6j). Interestingly, 10 W PN-DEX-M showed no changes in microglial morphology, gene expression, protein expression, or the HPA axis (Fig. S5a-j). These data show that the microglia of 10 W PN-DEX-F exhibited an inflammatory microglial phenotype.

Discussion

Maternal Gcs are transferred to the fetus through the placenta, and it has been reported that elevated maternal Gc levels are closely associated with the pathophysiology of several neuropsychiatric diseases in offspring [38]. In addition, neurodevelopmental changes, such as reduction of cortical thickness and changes in CNS-linked cell populations were observed following exposure of the fetal brain to prenatal DEX [39, 40].

Abnormal developmental programming of fetal microglia by *in utero* stress situations has been indicated as a key mechanism underlying abnormal brain development [41]. These *in utero* stress to fetal microglia including maternal immune challenges and maternal stress hormone induction alters microglial synaptic pruning and cytokine secretion and contributes to the prevalence of neuropsychiatric disorders such as major depressive disorder, and schizophrenia [42, 43].

Microglia also mediate several cellular functions, such as axon outgrowth, fasciculation, and cortical interneuron migration, during rodent fetal brain development between embryonic day14 (E14) and 17.5

(E17.5) [44]. Because neurogenesis in most cortical and subcortical regions begins on or around E9.5 [44, 45], we speculated that microglia-mediated synaptic formation and pruning that occurred during the perinatal period may have been induced by the DEX injected by us. Thus, exposure to DEX within the critical period of E15-E17, during maternity, may lead to a deterioration of brain development via microglial dysfunction. We also reported that DEX-treated fetal microglia displayed decreased phagocytic function, low proliferative capacity, and disrupted cytokine release, suggesting a dysfunctional state, such as cellular senescence, *in vitro* [46]. Therefore, DEX may disrupt normal microglial function, resulting in a state that is vulnerable to neuropsychiatric disorders.

Elevation of Gc-linked stress hormones during maternity may alter the cellular epigenetic landscape, including DNA methylation and histone acetylation in the CNS, thereby increasing its vulnerability to stress stimuli [4]. Exposure to stress during early life reportedly results in microglial DNA methylation in the STR and the HPC [47]. Glucocorticoid receptors (GRs) regulate a variety of genes via glucocorticoid response elements (GREs). Exposure to Gcs during fetal development induces epigenetic changes, including DNA methylation in GREs and other genes [48, 49]. Cytoplasmic GRs interacts with Gcs, resulting in the nuclear translocation of GRs and epigenetic modulation of the transcription of pro-/anti-inflammatory genes [50]. This indicates that stress-associated transcription, which is repressed by prenatal methylation of GRE, may be activated by demethylation of GRE via a second hit of Gc [51]. Additionally, FK506 binding protein 5, (FKBP5), which is an important modulator of the microglial stress response, regulates GR activity and its epigenetic modification by DEX [52]. A recent study revealed that epigenetic modification regulates microglial clearance in specific brain regions [53]. Considered together, these results indicate that exposure to DEX during maternity may lead to epigenetic modification of GRE-mediated transcription in the microglia of offspring, possibly accounting for the susceptibility to SCZ-relevant behavior in PN-DEX-M.

Perinatal androgen surge from the male testis and the subsequent local aromatization of testosterone to estradiol are crucial for the permanent modification of neuronal and microglial functions, as well as brain masculinization [54–56]. Testosterone surge during adolescence has been associated with several behavioral changes [57]. Progesterone, a testosterone precursor, antagonizes estradiol in synaptic remodeling, a process mediated by a progesterone receptor present on the microglia of rats [58]. In addition, several sex hormones, including estradiol and luteinizing hormone, are related to the onset of SCZ [59]. Thus, we speculated that the occurrence of SCZ-relevant behavior during the 10 W adult stage, but not during 5 W adolescent stage, may have been evoked by a pubertal testosterone surge which arose in response to the second Gc hit. However, our hypothesis was contradicted by the observation that testosterone depletion induced by orchiectomy did not prevent the occurrence of SCZ-relevant behavior in PN-DEX-M. Nevertheless, the possibility that other factors may have induced the second Gc hit and excessive microglial synaptic pruning cannot be discarded. Thus, further studies aimed at determining the possibility of a second Gc hit are felt to be warranted.

In our study, microglia in the STR and the mPFC of PN-DEX-M showed hyper-ramified morphology characterized by enlarged soma, as well as longer, more ramified branches at 10 W, but not at 5 W. These

morphological changes, which allowed their processes to extend toward neuronal synapses and engulf synaptic compartments, may have enabled aberrant synaptic pruning in 10 W PN-DEX males. The association of microglia with synaptic elimination and the regulation of neuronal activity via complement cascades has been known for many years [60–62]. It has been reported that increased expression of the complement 4 protein (C4) in the synapses of patients with SCZ in the pathological state, may enhance microglial synaptic pruning via complement receptor 3 (CR3). [63]. A previous study observed an increase in neuronal C1q and microglial CR3 expression during the elimination of unnecessary synapses during developmental stages [64]. However, 10 W PN-DEX-M showed a reduction in *C1qa* and *C3ar1* mRNA expression. We speculate that active synaptic pruning of microglia by the complement system may have been evoked after 5 W, but before 10 W, resulting in a reduction of the spine density of 10 W PN-DEX-M. In addition to the complement system, other genes are involved in synaptic pruning. Increased *Cd200r* expression in microglia affects their interaction with neurons as well as their homeostatic state [65]. *Cx3cr1* and *P2ry12* signaling, which direct microglial branches toward synaptic spines, are also involved in microglial synaptic pruning [66]. The results of the present study revealed that increased expression of *Cd200r* and *Cx3cr1* in 10 W PN-DEX-M was accompanied by ramified microglial morphology. This suggests that microglia may remain in a ramified state that enables them to easily contact neurons following aberrant synaptic pruning during adolescence. Considered together, these results suggest that changes in various genes associated with synaptic pruning in microglia, such *as C1qa, C3ar1, Cx3cr1, and P2ry12*, may have effected a decrease in synaptic density as well as pre-/post- synaptic protein expression in 10 W PN-DEX-M. Despite several genes in the striatum of 5 W/10 W PN-DEX males and females being altered, synaptic density remained unchanged. Microglial synaptic pruning is a sensory experience-dependent [67], as well as region- and time-dependent process [68]. This may explain the unchanged synaptic density seen in the STR. On the other hand, we found that the levels of DAT, TH, and DRD2 in the STR of 10 W PN-DEX males were significantly increased, whereas these proteins were decreased in the mPFC, suggesting the presence of hyperdopamine in the STR and hypo-dopamine in the mPFC. In summary, these data indicated that exposure to DEX during maternity induces SCZ-relevant behavior in male offspring via aberrant synaptic pruning and dysregulation of the dopamine system.

Depressive-like behavior observed in the 10 W PN-DEX-F group was accompanied by several changes in genes and proteins in the HPC. The expression levels of pro-inflammatory cytokine regulatory genes, including *Il1b, Il6*, and *Tnf-α*, in the HPC of this group were increased, while those of ARG-1 and CX3CR1 were slightly decreased. This suggests that prenatal DEX exposure induces inflammation in the HPC of female offspring via microglial activation. Similarly, hippocampal microglia show a pro-inflammatory phenotype and activated morphology, including enlarged soma as well as reduced branch length and arborization. Microglial activation may stimulate the HPA-axis, leading to increased hypothalamic Crh and serum Gc levels. Increased serum Gc levels caused by a chronically activated HPA axis may lead to GR insensitivity, which manifests in the form of decreased GR expression [69]. A decrease in ARG-1 positive microglia in the HPC is reportedly associated with depressive-like behavior [29], while an imbalance in the hypothalamic-pituitary-adrenal axis (HPA axis) was also found to be related to depressive-like behavior [29, 70]. These data provide mounting evidence supporting the previous

contention that cellular and molecular mechanisms may underly depression-like behavior. Hippocampal GR resistance (decreased GR expression) activates microglia, via decreased expression of ARG-1 and increased expression of pro-inflammatory genes, consequently aggravating HPA-axis imbalance (increased *Crh* and CORT) as well as depressive-like behavior [71]. Decreased hippocampal ARG-1 expression, in particular, may be associated with enhanced stress vulnerability [72].

A growing body of research indicates that early-life stress or prenatal stress may affect mouse and human behavior sex-dependently [73]. Biological gender has also been revealed to play a role in sex-dependent stress vulnerability and resilience to stress [74], brain sex differentiation via neuroimmunological function, and epigenetic modification [75]. Considering that developing microglia are closely associated with brain sex differentiation [76–78] and stress responses [74] during developmental stages, microglia may have acted as mediators of sex-specific behavior in the PN-DEX model. Several studies have suggested that microglia may display different functions [79], transcriptomes [80], and epigenetic landscapes depending on biological gender [55, 75]. Although considered as being supported by controversial evidence, differences in phagocytic functions and cytokine production have been discerned between male and female microglia [22].

In our prenatal DEX regimen, only 10 W PN-DEX-F showed HPA activation. HPA-axis activation which occurs exclusively in females may be associated with differences in the distribution of GR isoforms in the male placenta. In addition, synthetic Gcs and DEX evidently modulate GR expression only in female placentas [81]. The results of our study suggest that sex-differential distribution of GR isoforms in the placenta may explain the sex-biased behavior and HPA-axis programming evoked by the PN-DEX regimen. Therefore, we speculate that sex-dependent placental GR signaling and sex-dependent microglial development may have led to sex-dependent behavior in offspring following exposure to DEX during maternity.

Conclusion

The current study demonstrated that maternal DEX exposure induces sex-biased abnormal behavior, such as SCZ-relevant behavior in male offspring, and depressive-like behavior in female offspring. In addition, we propose that altered microglial functions, such as synaptic pruning, may be involved in the occurrence of SCZ-relevant behavior in PN-DEX-M. However, the following issues remain unresolved: (i) the nature of the association between the second Gc hit and microglial functional changes that led to SCZ-relevant behaviors seen only in 10 W PN-DEX-M; and (ii) the mechanism underlying sex-dependent differentiation of disease phenotypes in PN-DEX offspring. Thus, further studies using the PN-DEX model may be required to address these issues.

Abbreviations

DEX: Dexamethasone, 10W: 10 week old (adult) 5W: 5 week old (adolescence), mPFC: Medial prefrontal cortex, STR: Striatum, PSD95: Post-synaptic density 95, PN-DEX: Prenatally treated with dexamethasone,

PN-DEX-F: Female with prenatally dexamethasone exposure. PN-DEX-M: Male with prenatally dexamethasone exposure, HPC: Hippocampus, SCZ: Schizophrenia, HPA axis: Hypothalamic-pituitary-adrenal axis, CNS: Central nervous system, Gc: Glucocorticoid, VTA: Ventral tegmental area, PFC: Prefrontal cortex, DRD1/DRD2: Dopamine receptor D1/D2, MSN: Medium spiny neuron, GD: Gestational day, TST: Tail suspension test, SPT: Sucrose preference test, PPI: Prepulse inhibition, SI: Social interaction, FST: Forced swimming test, LD: Light dart exploration, LI: Latent inhibition, AMP: Amphetamine, Veh: Vehicle group (Non-prenatally dexamethasone exposed group), DAT: Dopamine transporter, TH: Tyrosine hydroxylase, Physin: Synaptophysin, IBA1: Ionized calcium-binding adapter molecule 1, Orx: Orchiectomy, GR: Glucocorticoid receptor, GRE: Glucocorticoid response element, CR3: Complement receptor 3, ARG-1: Arginase 1, CORT: Corticosterone.

Declarations

Ethical Approval and consent to participate

All experimental animals were handled in accordance with the guidelines of the Institutional Animal Care and Use Committee of CHA University (IACUC2100037).

Consent for publication

Not applicable.

Availability of data and materials

The data are available upon request.

Competing interests

All authors declare that they have no competing interests.

Funding

This research was supported by the National Research Foundation of Korea (NRF) grant funded by the Korean Government (MIST) (2021M3E5D9025027).

Author contributions

C Rim and HS Park performed the experiments and wrote the manuscript. MJ You and B Yang performed morphological analysis independently. HJ Kim and S Sung conducted behavioral study. MS Kwon directed the overall study, including designing the experiments, analyzing the data, and writing the manuscript. All authors read and approved the final manuscript.

Acknowledgments

Not applicable

References

1. Kahn RS, Sommer IE, Murray RM, Meyer-Lindenberg A, Weinberger DR, Cannon TD, O'Donovan M, Correll CU, Kane JM, Os Jv, Insel TR: Schizophrenia. Nature Reviews Disease Primers 2015, 1:15067.
2. Riecher-Rössler A: Oestrogens, prolactin, hypothalamic-pituitary-gonadal axis, and schizophrenic psychoses. The Lancet Psychiatry 2017, 4:63–72.
3. Moore H, Susser E: Relating the effects of prenatal stress in rodents to the pathogenesis of schizophrenia. Biol Psychiatry 2011, 70:906–907.
4. Krontira AC, Cruceanu C, Binder EB: Glucocorticoids as Mediators of Adverse Outcomes of Prenatal Stress. Trends in Neurosciences 2020, 43:394–405.
5. Cserép C, Pósfai B, Dénes Á: Shaping Neuronal Fate: Functional Heterogeneity of Direct Microglia-Neuron Interactions. Neuron 2020, 109:222–240.
6. Butovsky O, Weiner HL: Microglial signatures and their role in health and disease. Nature Reviews Neuroscience 2018, 19:622–635.
7. Lenz KM, Nelson LH: Microglia and Beyond: Innate Immune Cells As Regulators of Brain Development and Behavioral Function. Front Immunol 2018, 9:698.
8. Prinz M, Priller J: Microglia and brain macrophages in the molecular age: from origin to neuropsychiatric disease. Nature Reviews Neuroscience 2014, 15:300–312.
9. Yao WD, Spealman RD, Zhang J: Dopaminergic signaling in dendritic spines. Biochem Pharmacol 2008, 75:2055–2069.
10. Sellgren CM, Sheridan SD, Gracias J, Xuan D, Fu T, Perlis RH: Patient-specific models of microglia-mediated engulfment of synapses and neural progenitors. Molecular Psychiatry 2017, 22:170–177.
11. Sellgren CM, Gracias J, Watmuff B, Biag JD, Thanos JM, Whittredge PB, Fu T, Worringer K, Brown HE, Wang J, et al: Increased synapse elimination by microglia in schizophrenia patient-derived models of synaptic pruning. Nature Neuroscience 2019, 22:374–385.
12. Peter H: Synaptic density in human frontal cortex — Developmental changes and effects of aging. Brain Research 1979, 163:195–205.
13. Beggs S, Salter MW: SnapShot: Microglia in Disease. Cell 2016, 165:1294–1294 e1291.
14. Robison AJ, Thakkar KN, Diwadkar VA: Cognition and Reward Circuits in Schizophrenia: Synergistic, Not Separate. Biol Psychiatry 2020, 87:204–214.
15. McCutcheon RA, Abi-Dargham A, Howes OD: Schizophrenia, Dopamine and the Striatum: From Biology to Symptoms. Trends Neurosci 2019, 42:205–220.
16. Quessy F, Bittar T, Blanchette LJ, Levesque M, Labonte B: Stress-induced alterations of mesocortical and mesolimbic dopaminergic pathways. Sci Rep 2021, 11:11000.
17. Arnsten AF: Stress signalling pathways that impair prefrontal cortex structure and function. Nat Rev Neurosci 2009, 10:410–422.

18. Selemon LD, Zecevic N: Schizophrenia: a tale of two critical periods for prefrontal cortical development. Translational Psychiatry 2015, 5:e623-e623.
19. Simpson EH, Kellendonk C, Kandel E: A possible role for the striatum in the pathogenesis of the cognitive symptoms of schizophrenia. Neuron 2010, 65:585–596.
20. Zhang YQ, Lin WP, Huang LP, Zhao B, Zhang CC, Yin DM: Dopamine D2 receptor regulates cortical synaptic pruning in rodents. Nat Commun 2021, 12:6444.
21. Lenz KM, McCarthy MM: A starring role for microglia in brain sex differences. Neuroscientist 2015, 21:306–321.
22. Han J, Fan Y, Zhou K, Blomgren K, Harris RA: Uncovering sex differences of rodent microglia. Journal of Neuroinflammation 2021, 18:74.
23. Villa A, Gelosa P, Castiglioni L, Cimino M, Rizzi N, Pepe G, Lolli F, Marcello E, Sironi L, Vegeto E, Maggi A: Sex-Specific Features of Microglia from Adult Mice. Cell Reports 2018, 23:3501–3511.
24. Bollinger JL: Uncovering microglial pathways driving sex-specific neurobiological effects in stress and depression. *Brain, Behavior, & Immunity - Health* 2021, 16:100320.
25. Nagano M, Ozawa H, Suzuki H: Prenatal dexamethasone exposure affects anxiety-like behaviour and neuroendocrine systems in an age-dependent manner. Neurosci Res 2008, 60:364–371.
26. Han A, Yeo H, Park M-J, Kim SH, Choi HJ, Hong C-W, Kwon M-S: IL-4/10 prevents stress vulnerability following imipramine discontinuation. Journal of Neuroinflammation 2015, 12:197.
27. You M-J, Bang M, Park H-S, Yang B, Jang KB, Yoo J, Hwang D-Y, Kim M, Kim B, Lee S-H, Kwon M-S: Human umbilical cord-derived mesenchymal stem cells alleviate schizophrenia-relevant behaviors in amphetamine-sensitized mice by inhibiting neuroinflammation. Translational Psychiatry 2020, 10:123.
28. Smith SE, Li J, Garbett K, Mirnics K, Patterson PH: Maternal immune activation alters fetal brain development through interleukin-6. J Neurosci 2007, 27:10695–10702.
29. Yang B, Ryu J-S, Rim C, Shin JU, Kwon M-S: Possible role of arginase 1 positive microglia on depressive/anxiety-like behaviors in atopic dermatitis mouse model. Archives of Pharmacal Research 2022, 45:11–28.
30. Danielson E, Lee SH: SynPAnal: Software for Rapid Quantification of the Density and Intensity of Protein Puncta from Fluorescence Microscopy Images of Neurons. PLOS ONE 2014, 9:e115298.
31. Cardozo PL, de Lima IBQ, Maciel EMA, Silva NC, Dobransky T, Ribeiro FM: Synaptic Elimination in Neurological Disorders. Curr Neuropharmacol 2019, 17:1071–1095.
32. Young K, Morrison H: Quantifying Microglia Morphology from Photomicrographs of Immunohistochemistry Prepared Tissue Using ImageJ. J Vis Exp 2018.
33. Derecki N, Norris G, Kipnis J: Microglial Sholl Analysis. Protocol Exchange 2014.
34. Marquand AF, Haak KV, Beckmann CF: Functional corticostriatal connection topographies predict goal directed behaviour in humans. Nat Hum Behav 2017, 1:0146.

35. Yan Z, Rein B: Mechanisms of synaptic transmission dysregulation in the prefrontal cortex: pathophysiological implications. Mol Psychiatry 2022, 27:445–465.
36. Ott T, Nieder A: Dopamine and Cognitive Control in Prefrontal Cortex. Trends Cogn Sci 2019, 23:213–234.
37. Kopec AM, Smith CJ, Ayre NR, Sweat SC, Bilbo SD: Microglial dopamine receptor elimination defines sex-specific nucleus accumbens development and social behavior in adolescent rats. Nat Commun 2018, 9:3769.
38. Seckl JR, Holmes MC: Mechanisms of disease: glucocorticoids, their placental metabolism and fetal 'programming' of adult pathophysiology. Nat Clin Pract Endocrinol Metab 2007, 3:479–488.
39. Davis EP, Sandman CA, Buss C, Wing DA, Head K: Fetal glucocorticoid exposure is associated with preadolescent brain development. Biol Psychiatry 2013, 74:647–655.
40. Noorlander CW, Tijsseling D, Hessel EV, de Vries WB, Derks JB, Visser GH, de Graan PN: Antenatal glucocorticoid treatment affects hippocampal development in mice. PLoS One 2014, 9:e85671.
41. Ceasrine AM, Batorsky R, Shook LL, Kislal S, Bordt EA, Devlin BA, Perlis RH, Slonim DK, Bilbo SD, Edlow AG: Single cell profiling of Hofbauer cells and fetal brain microglia reveals shared programs and functions. *bioRxiv* 2021:2021.2012.2003.471177.
42. Hanamsagar R, Bilbo SD: Environment matters: microglia function and dysfunction in a changing world. Current Opinion in Neurobiology 2017, 47:146–155.
43. Tay TL, Béchade C, D'Andrea I, St-Pierre M-K, Henry MS, Roumier A, Tremblay M-E: Microglia Gone Rogue: Impacts on Psychiatric Disorders across the Lifespan. Frontiers in Molecular Neuroscience 2018, 10:421.
44. Thion MS, Ginhoux F, Garel S: Microglia and early brain development: An intimate journey. Science 2018, 362:185–189.
45. Semple BD, Blomgren K, Gimlin K, Ferriero DM, Noble-Haeusslein LJ: Brain development in rodents and humans: Identifying benchmarks of maturation and vulnerability to injury across species. Prog Neurobiol 2013, 106–107:1–16.
46. Park M-J, Park H-S, You M-J, Yoo J, Kim SH, Kwon M-S: Dexamethasone Induces a Specific Form of Ramified Dysfunctional Microglia. Molecular Neurobiology 2019, 56:1421–1436.
47. Catale C, Bussone S, Lo Iacono L, Viscomi MT, Palacios D, Troisi A, Carola V: Exposure to different early-life stress experiences results in differentially altered DNA methylation in the brain and immune system. Neurobiol Stress 2020, 13:100249.
48. Wiechmann T, Roh S, Sauer S, Czamara D, Arloth J, Kodel M, Beintner M, Knop L, Menke A, Binder EB, Provencal N: Identification of dynamic glucocorticoid-induced methylation changes at the FKBP5 locus. Clin Epigenetics 2019, 11:83.
49. Provencal N, Arloth J, Cattaneo A, Anacker C, Cattane N, Wiechmann T, Roh S, Kodel M, Klengel T, Czamara D, et al: Glucocorticoid exposure during hippocampal neurogenesis primes future stress response by inducing changes in DNA methylation. Proc Natl Acad Sci U S A 2020, 117:23280–23285.

50. Gerber AN, Newton R, Sasse SK: Repression of transcription by the glucocorticoid receptor: A parsimonious model for the genomics era. J Biol Chem 2021, 296:100687.
51. Thomassin H, Flavin M, Espinás ML, Grange T: Glucocorticoid-induced DNA demethylation and gene memory during development. The EMBO Journal 2001, 20:1974–1983.
52. Yeh H, Ikezu T: Transcriptional and Epigenetic Regulation of Microglia in Health and Disease. Trends Mol Med 2019, 25:96–111.
53. Ayata P, Badimon A, Strasburger HJ, Duff MK, Montgomery SE, Loh Y-HE, Ebert A, Pimenova AA, Ramirez BR, Chan AT, et al: Epigenetic regulation of brain region-specific microglia clearance activity. Nature neuroscience 2018, 21:1049–1060.
54. Arnold AP, Gorski RA: Gonadal Steroid Induction of Structural Sex Differences in the Central Nervous System. Annual Review of Neuroscience 1984, 7:413–442.
55. Nugent BM, Wright CL, Shetty AC, Hodes GE, Lenz KM, Mahurkar A, Russo SJ, Devine SE, McCarthy MM: Brain feminization requires active repression of masculinization via DNA methylation. Nature neuroscience 2015, 18:690–697.
56. Villa A, Vegeto E, Poletti A, Maggi A: Estrogens, Neuroinflammation, and Neurodegeneration. Endocrine Reviews 2016, 37:372–402.
57. Peper JS, Dahl RE: Surging Hormones: Brain-Behavior Interactions During Puberty. Curr Dir Psychol Sci 2013, 22:134–139.
58. Kato TA, Hayakawa K, Monji A, Kanba S: Missing and Possible Link between Neuroendocrine Factors, Neuropsychiatric Disorders, and Microglia. Front Integr Neurosci 2013, 7:53.
59. Gogos A, Sbisa AM, Sun J, Gibbons A, Udawela M, Dean B: A Role for Estrogen in Schizophrenia: Clinical and Preclinical Findings. *Int J Endocrinol* 2015, 2015:615356.
60. Stevens B, Allen NJ, Vazquez LE, Howell GR, Christopherson KS, Nouri N, Micheva KD, Mehalow AK, Huberman AD, Stafford B, et al: The classical complement cascade mediates CNS synapse elimination. Cell 2007, 131:1164–1178.
61. Wake H, Moorhouse AJ, Jinno S, Kohsaka S, Nabekura J: Resting microglia directly monitor the functional state of synapses in vivo and determine the fate of ischemic terminals. J Neurosci 2009, 29:3974–3980.
62. Schafer DP, Lehrman EK, Kautzman AG, Koyama R, Mardinly AR, Yamasaki R, Ransohoff RM, Greenberg ME, Barres BA, Stevens B: Microglia sculpt postnatal neural circuits in an activity and complement-dependent manner. Neuron 2012, 74:691–705.
63. Comer AL, Jinadasa T, Sriram B, Phadke RA, Kretsge LN, Nguyen TPH, Antognetti G, Gilbert JP, Lee J, Newmark ER, et al: Increased expression of schizophrenia-associated gene C4 leads to hypoconnectivity of prefrontal cortex and reduced social interaction. PLOS Biology 2020, 18:e3000604.
64. Thion MS, Garel S: Microglia Under the Spotlight: Activity and Complement-Dependent Engulfment of Synapses. Trends Neurosci 2018, 41:332–334.

65. Manich G, Recasens M, Valente T, Almolda B, Gonzalez B, Castellano B: Role of the CD200-CD200R Axis During Homeostasis and Neuroinflammation. Neuroscience 2019, 405:118–136.
66. Sipe GO, Lowery RL, Tremblay ME, Kelly EA, Lamantia CE, Majewska AK: Microglial P2Y12 is necessary for synaptic plasticity in mouse visual cortex. Nat Commun 2016, 7:10905.
67. Holtmaat A, Svoboda K: Experience-dependent structural synaptic plasticity in the mammalian brain. Nature Reviews Neuroscience 2009, 10:647–658.
68. Geloso MC, D'Ambrosi N: Microglial Pruning: Relevance for Synaptic Dysfunction in Multiple Sclerosis and Related Experimental Models. Cells 2021, 10:686.
69. Lupien SJ, McEwen BS, Gunnar MR, Heim C: Effects of stress throughout the lifespan on the brain, behaviour and cognition. Nat Rev Neurosci 2009, 10:434–445.
70. Krishnan V, Nestler EJ: The molecular neurobiology of depression. Nature 2008, 455:894–902.
71. Park H-S, You M-J, Yang B, Jang KB, Yoo J, Choi HJ, Lee S-H, Bang M, Kwon M-S: Chronically infused angiotensin II induces depressive-like behavior via microglia activation. Scientific Reports 2020, 10:22082.
72. Zhang J, Rong P, Zhang L, He H, Zhou T, Fan Y, Mo L, Zhao Q, Han Y, Li S, et al: IL4-driven microglia modulate stress resilience through BDNF-dependent neurogenesis. Science Advances 2021, 7:eabb9888.
73. Reshetnikov VV, Ayriyants KA, Ryabushkina YA, Sozonov NG, Bondar NP: Sex-specific behavioral and structural alterations caused by early-life stress in C57BL/6 and BTBR mice. Behavioural Brain Research 2021, 414:113489.
74. Hodes GE, Epperson CN: Sex Differences in Vulnerability and Resilience to Stress Across the Life Span. Biological Psychiatry 2019, 86:421–432.
75. McCarthy MM, Nugent BM, Lenz KM: Neuroimmunology and neuroepigenetics in the establishment of sex differences in the brain. Nature Reviews Neuroscience 2017, 18:471–484.
76. Bordt EA, Ceasrine AM, Bilbo SD: Microglia and sexual differentiation of the developing brain: A focus on ontogeny and intrinsic factors. Glia 2020, 68:1085–1099.
77. VanRyzin JW, Marquardt AE, Pickett LA, McCarthy MM: Microglia and sexual differentiation of the developing brain: A focus on extrinsic factors. Glia 2020, 68:1100–1113.
78. VanRyzin JW, Pickett LA, McCarthy MM: Microglia: Driving critical periods and sexual differentiation of the brain. Developmental Neurobiology 2018, 78:580–592.
79. Bordeleau M, Carrier M, Luheshi GN, Tremblay M-È: Microglia along sex lines: From brain colonization, maturation and function, to implication in neurodevelopmental disorders. Seminars in Cell & Developmental Biology 2019, 94:152–163.
80. Guneykaya D, Ivanov A, Hernandez DP, Haage V, Wojtas B, Meyer N, Maricos M, Jordan P, Buonfiglioli A, Gielniewski B, et al: Transcriptional and Translational Differences of Microglia from Male and Female Brains. Cell Reports 2018, 24:2773–2783.e2776.

81. Cuffe JSM, Saif Z, Perkins AV, Moritz KM, Clifton VL: Dexamethasone and sex regulate placental glucocorticoid receptor isoforms in mice. Journal of Endocrinology 2017, 234:89–100.

Figures

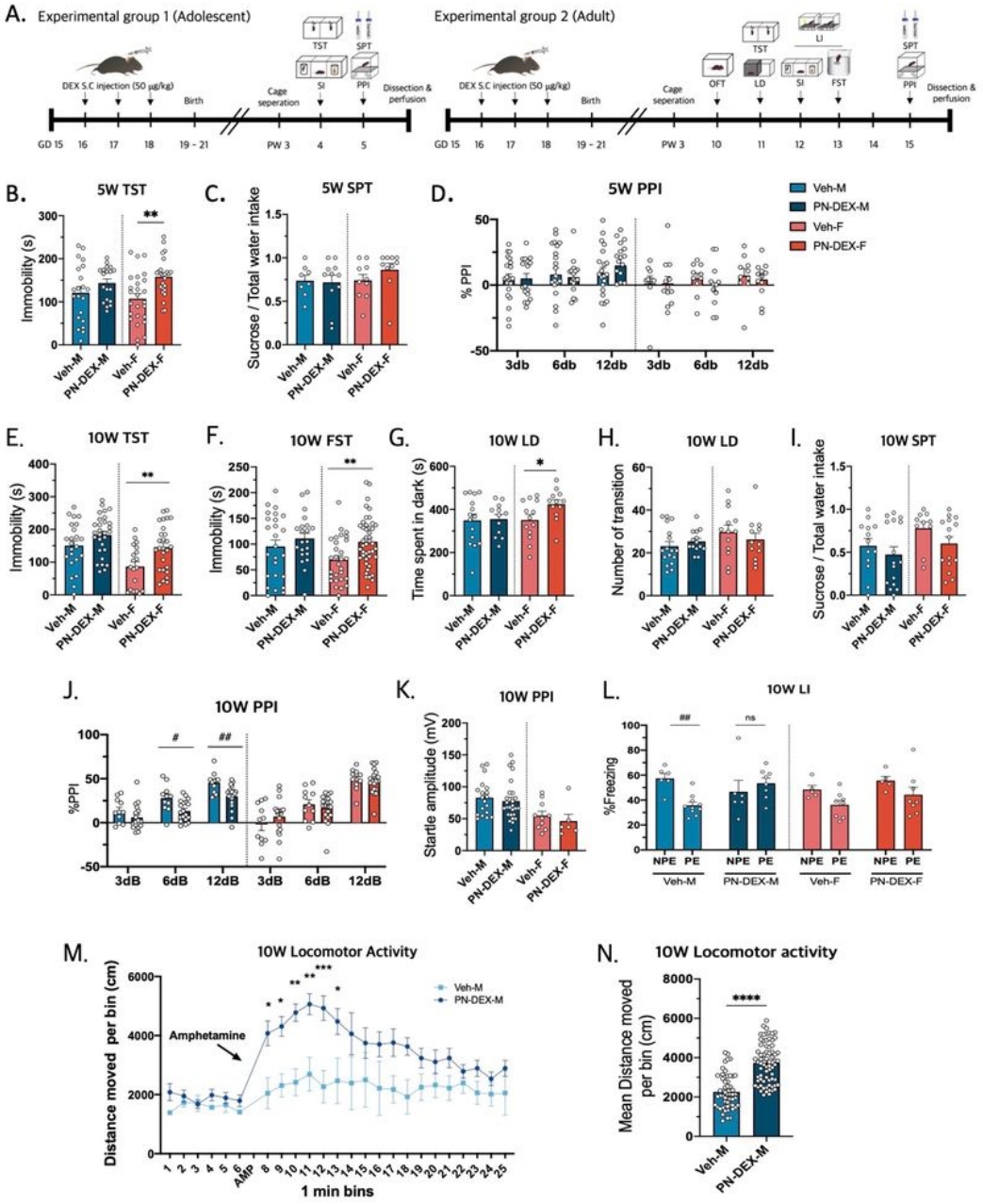

Fig 1. Maternal dexamethasone exposure induces sex-different behaviors in offspring
(A) Maternal dexamethasone exposure regimen: Dexamethasone (50 µg/kg) was subcutaneously injected into dams between gestational days 15 and 17, and a series of behavioral assessments were conducted in the offspring. (B) The 5 W PN-DEX-F showed increased immobility time in the TST. (C) No change in sucrose consumption was observed in any experimental group. (D) All experimental groups showed intact sensory gating functions at 3, 6, and 12 dB. (E) The 10 W PN-DEX-F showed increased immobility time in the TST and (F) FST. (G-H) 10 W PN-DEX-F showed increased dwelling time in the dark area in the LD test. (I) No significant changes were observed between sucrose consumption in the 10 W PN-DEX group and the 10 W Veh group. (J-K) 10 W PN-DEX-M showed significantly impaired sensory gating function in PPI but not in startle amplitude. (L) 10 W PN-DEX-M showed impaired LI. (M-N) Locomotor activity after amphetamine injection was increased. Data are presented as mean ± standard error of the mean (SEM). For the TST, FST, LD, SPT, and locomotor activity, an unpaired t-test was conducted. * = $p < 0.05$, ** = $p < 0.01$ compared with the Veh-M and Veh-F independently. For PPI and LI, two-way ANOVA followed by Tukey's post-test was conducted; # = $p < 0.05$, ## = $p < 0.01$.

Figure 1

See image above for figure legend.

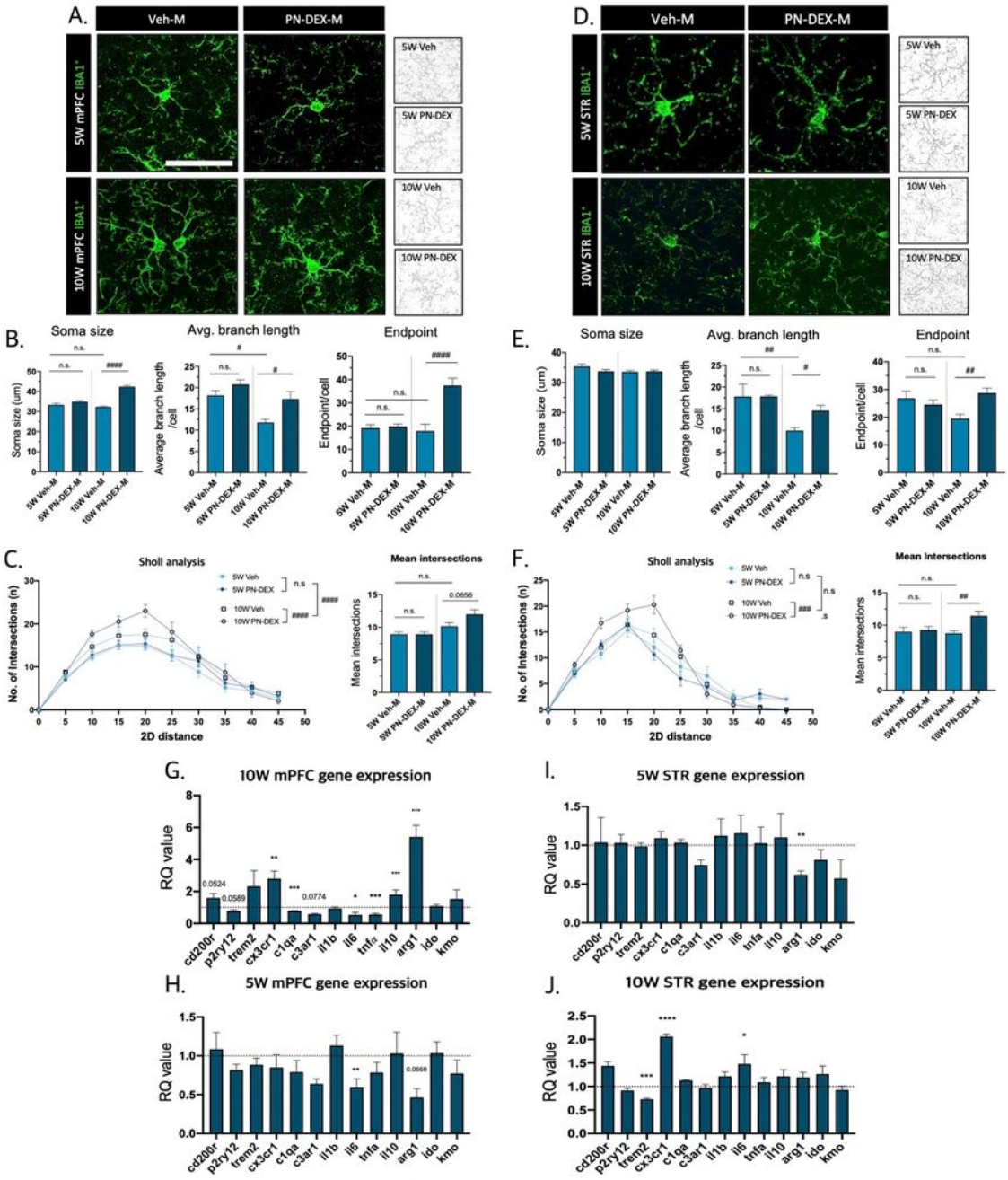

Fig 2. Maternal dexamethasone exposure induces microglial changes in the mPFC and the striatum of offspring
(A) Representative images of the morphology of Iba-1 positive cells in the medial prefrontal cortex (mPFC) according to time point and sex. (B) Soma size, branch length, and the number of endpoints in Iba-1 positive cells in the mPFC were calculated. (C) Sholl analysis indicated that mPFC microglia had a hyper-ramified morphology. (D) Representative images of the morphology of Iba-1 positive cells in the striatum (STR) according to time point and sex. (E) Soma size, branch length, and number of endpoints of Iba-1 positive cells in the STR were calculated. (F) Sholl analysis showed that striatal microglia had a hyper-ramified morphology. (G) qRT-PCR analysis to determine gene expression patterns in the mPFC of 5 W PN-DEX-M compared to that of 5 W Veh-M, and (H) the mPFC of 10 W PN-DEX-M compared to that of 10 W Veh-M. (I) 5 W PN-DEX-M STR, (J) 10 W PN-DEX-M STR. The RQ values are the ratios of the respective genes as a percentage of Veh. Data are presented as mean ± standard error of the mean (SEM). An unpaired t-test was used for qRT-PCR; * = $p < 0.05$, ** = $p < 0.01$, and *** = $p < 0.001$ compared with the Veh-M and Veh-F independently, For morphology analysis, two-way ANOVA followed by Tukey's post-test was conducted; # = $p < 0.05$, ## = $p < 0.01$, and #### = $p < 0.0001$.

Figure 2

See image above for figure legend.

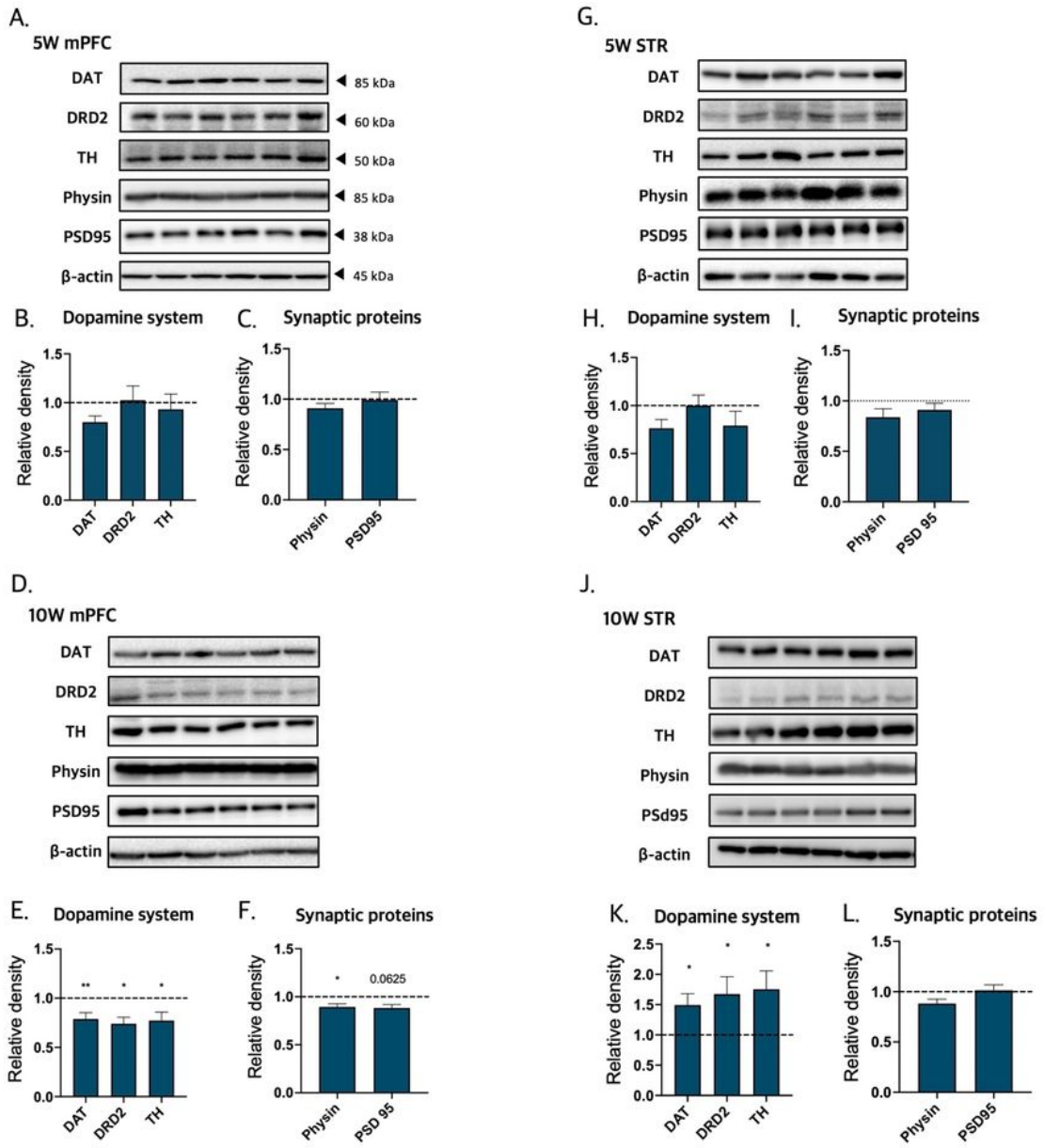

Figure 3. Change in synaptic protein and the dopamine system in male offspring with maternal dexamethasone exposure
Dopamine-related and synaptic protein levels were assessed via western blot analysis, and their expression was quantified using ImageJ. Relative density is defined as the ratio of respective protein density as a percentage of beta-actin density. (A) Representative bands of dopamine-related proteins and synaptic proteins in the 5 W mPFC. (B) Quantification of the relative density of dopamine-related proteins. (C) synaptic proteins in the 5 W mPFC. (D) representative band of dopamine-related protein and synaptic protein in the 10 W mPFC. (E) Quantification of the relative density of dopamine-related proteins and (F) synaptic proteins in the 10 W mPFC. (G) Representative bands of dopamine-related proteins and synaptic proteins in the 5 W STR. (H) Quantification of the relative density of dopamine-related proteins and (I) synaptic proteins in the 5 W STR. (J) Representative band of dopamine-related and synaptic proteins in the 10 W STR. (K) Quantification of the relative density of dopamine-related proteins and (L) synaptic proteins in the 10 W STR. The data are shown as mean ± standard error of the mean (SEM). For the purpose of statistical analyses, we conducted an unpaired t-test; * = $p < 0.05$, and ** = $p < 0.01$, compared with Veh-M.

Figure 3

See image above for figure legend.

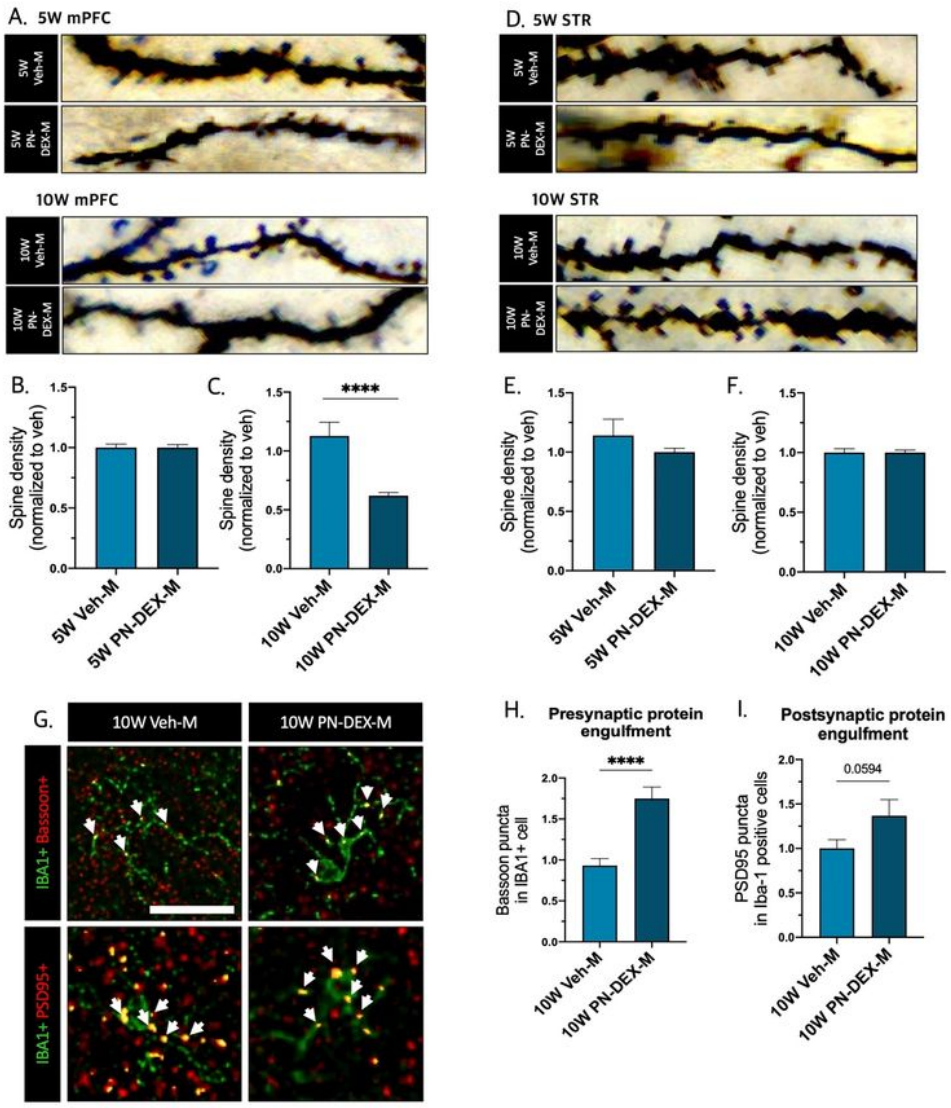

Figure 4. Increased microglia engulfment of pre-/post-synaptic proteins in the mPFC of 10 W PN-DEX-M
(A) Representative images of Golgi staining used to calculate spine density in 5 W and 10 W mPFC. (B) Spine density of 5W PN-DEX-M mPFC, and (C) 10W PN-DEX-M mPFC, normalized to the spine density of Veh-M. (D) Representative images of Golgi staining used to calculate spine density in 5 W and 10 W STR. (E) Spine density of 5 W PN-DEX-M STR, and (F) 10 W PN-DEX-M STR, normalized to the spine density of Veh-M. (G) Representative images of Bassoon (presynaptic marker) and PSD95 (post-synaptic) colocalized with Iba-1 positive cells in 10 W mPFC. (H-I). Quantification of Bassoon and PSD95 puncta in Iba-1 positive cells of 10 W mPFC. Data are presented as mean ± standard error of the mean (SEM), For the purpose of statistical analysis, we conducted an unpaired t-test; *** = $p < 0.001$, and **** = $p < 0.0001$, compared with the Veh-M.

Figure 4

See image above for figure legend.

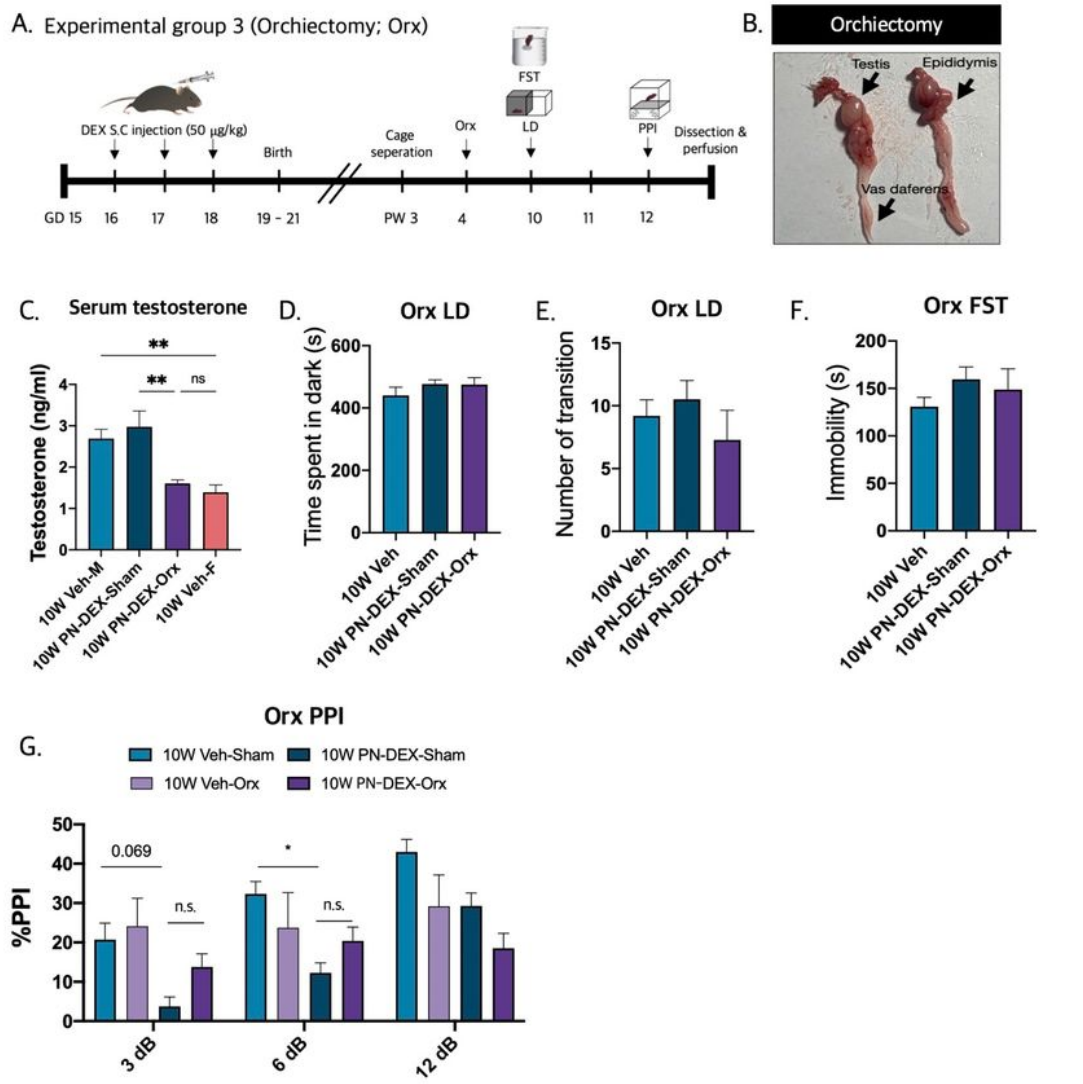

Figure 5. Testosterone surge in adolescent period is not related to the occurrence of schizophrenia-relevant behaviors with maternal dexamethasone exposure

(A) Experimental scheme for behavioral assessment following orchiectomy. (B) Representative images of dissected orchiectomy tissues. (C) Serum testosterone levels decrease after orchiectomy. (D-E) There were no significant behavioral changes in the LD, (F) FST, and (G) PPI groups. The data are expressed as the mean ± standard error of the mean (SEM), and one-way ANOVA followed by Tukey's post-test was conducted; * = $p < 0.05$; ** = $p < 0.01$.

Figure 5

See image above for figure legend.

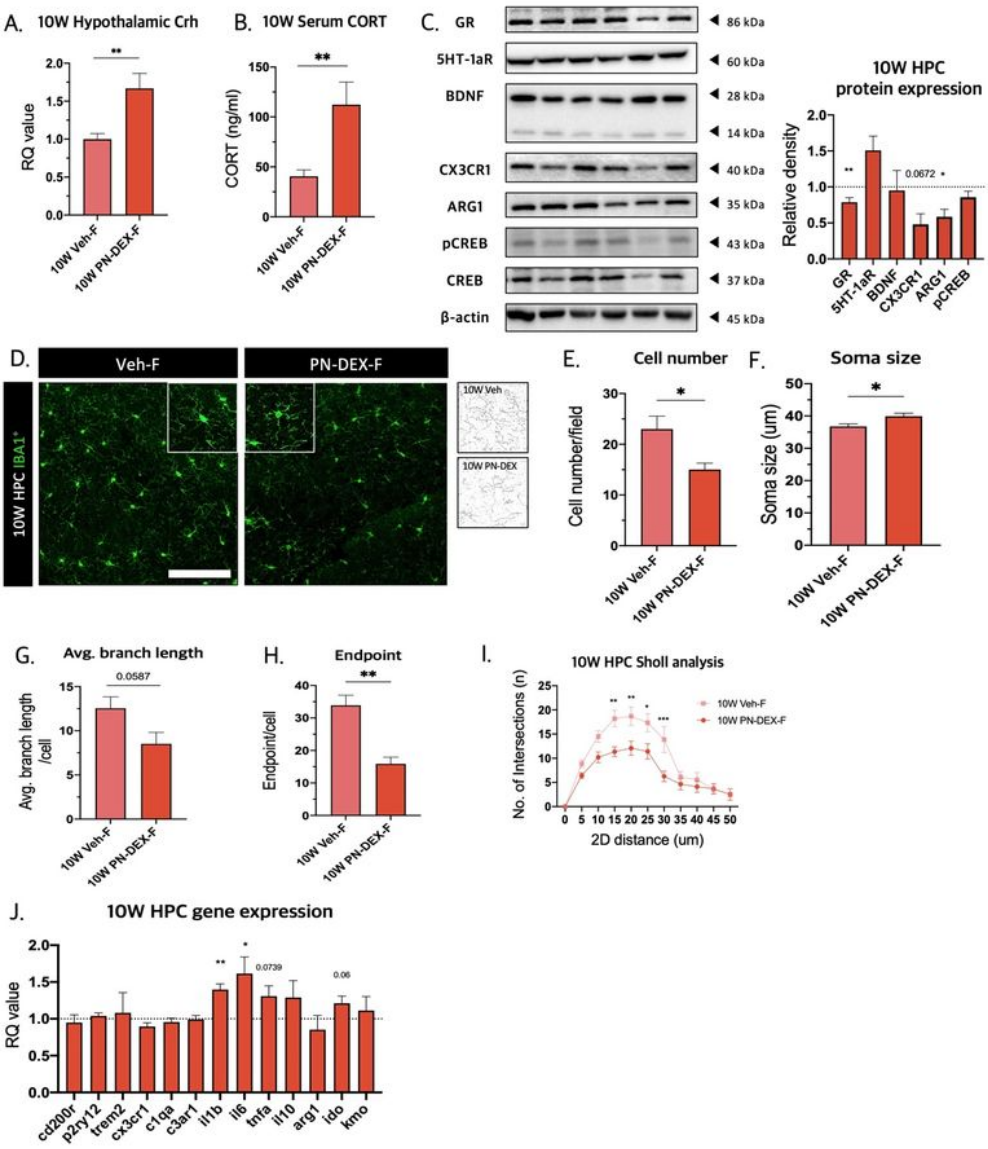

Figure 6. PN-DEX-F showed HPA axis activation and inflammatory microglia phenotype in the hippocampus

(A) Hypothalamic Crh levels were measured using qRT-PCR. (B) Serum corticosterone levels were measured using ELISA. (C) Western blotting was used to assess several proteins related to depression-like behavior. Relative density is defined as the ratio of respective protein density as a percentage of β-actin density. (D) Representative images of Iba-1 positive cells in the hippocampus and skeletonized images (40x image, scale bar = 100 µm). (E) Cell number, (F) soma size, (G) branch length, and (H) number of endpoints in the HPC microglia. (I) Sholl analysis showed that hippocampal microglia displayed de-ramified morphology. (J) qRT-PCR analysis used to determine gene expression patterns in 10 W PN-DEX-F HPC compared to 10 W Veh-F. Data are expressed as the mean ± standard error of the mean (SEM), and two-way ANOVA followed by Tukey's post-test. Was conducted; # = $p < 0.05$, ## = $p < 0.01$, and ### = $p < 0.001$. For the unpaired t-test, * = $p < 0.05$, ** = $p < 0.01$, compared with Veh-F.

Figure 6

See image above for figure legend.

Supplementary Files

This is a list of supplementary files associated with this preprint. Click to download.

- SupplementaryMaterial.docx